Journal of *Marine Science and Engineering*

MDPI

Article

Real-Time Fault Diagnosis of Mooring Chain Jack Hydraulic System Based on Multi-Scale Feature Fusion Under Diverse Operating Conditions

Yujia Liu [1,2,3], Wenhua Li [1,2,3,*], Haoran Ye [1,2,3], Shanying Lin [1,2,3] and Lei Hong [4]

[1] Marine Engineering College, Dalian Maritime University, Dalian 116026, China; lyj1118@dlmu.edu.cn (Y.L.); yehr@dlmu.edu.cn (H.Y.); linsy@dlmu.edu.cn (S.L.)
[2] State Key Laboratory of Maritime Technology and Safety, Dalian 116026, China
[3] National Center for International Research of Subsea Engineering Technology and Equipment, Dalian Maritime University, Dalian 116026, China
[4] Nantong Liwei Machinery Co., Ltd., Nantong 226522, China; jshlit@163.com
* Correspondence: lwh992@dlmu.edu.cn

Abstract: The condition monitoring of mooring equipment is an important engineering reliability issue during the operation of a floating production storage and offloading unit (FPSO). The chain jack (CJ) is the key equipment for powering the mooring chain in a spread mooring system. Under complex and dynamic marine operating conditions, different severity faults in the CJ hydraulic system display distinct time-scale characteristics. Hence, this paper proposes a real-time fault diagnosis method of the CJ hydraulic system based on multi-scale feature fusion. Firstly, the model incorporates a convolutional neural network (CNN) layer to extract localized spatial features from multivariate time-series data, effectively identifying fault patterns over the associated short intervals. Subsequently, the bidirectional long short-term memory (BiLSTM) layer is introduced to construct a dynamic temporal model to comprehensively capture the evolution of the fault severity. Finally, a multi-scale global attention mechanism (GAM) emphasizes persistent fault behaviors across time scales, dynamically prioritizing relevant features to improve diagnostic accuracy and model interpretability. The study results indicate that the proposed model's accuracy improves by 7.36% over the CNN-GAM for 11 failure modes, up to 99.34%. This study contributes to the safe operation of an FPSO by guiding monitoring CJ operations under different load conditions.

Keywords: floating production storage and offloading; chain jack; hydraulic system; fault diagnosis; bidirectional long short-term memory; global attention mechanism

check for updates

Academic Editor: Giuseppe Giorgi

Received: 27 February 2025
Revised: 25 March 2025
Accepted: 13 April 2025
Published: 15 April 2025

Citation: Liu, Y.; Li, W.; Ye, H.; Lin, S.; Hong, L. Real-Time Fault Diagnosis of Mooring Chain Jack Hydraulic System Based on Multi-Scale Feature Fusion Under Diverse Operating Conditions. *J. Mar. Sci. Eng.* **2025**, *13*, 783. https://doi.org/10.3390/jmse13040783

Copyright: © 2025 by the authors. Licensee MDPI, Basel, Switzerland. This article is an open access article distributed under the terms and conditions of the Creative Commons Attribution (CC BY) license (https://creativecommons.org/licenses/by/4.0/).

1. Introduction

A spread mooring system is crucial for the safe operation of a floating production storage and offloading (FPSO) platform without power drive [1,2]. The windlasses and winches are commonly used as chain retraction equipment in traditional mooring systems. Due to low automation and excessive bending stress, the chain is seriously worn. Therefore, the hydraulic synchronized CJ is widely used in the FPSO mooring system. Wudtke [3] developed a linear vertical lifting anchor chain hoist to replace the traditional FPSO mooring system, reducing the investment cost. Grindheim [4] took the GOLIAT project of ENI Group and the P58/P62 project of PETROBRAS as examples and introduced in detail the difference between the movable anchor system and the movable CJ. Wang et al. [5] used the CJ to keep the relative static between the two yoke arms during the operation of the rotating soft yoke

mooring system and the FPSO, which was convenient for docking installation. Biggerstaff et al. [6] discussed the design, manufacture and installation of 1000 tons of CJs. The offshore installation of Lucius Spar export risers was completed by using the installed CJ. Sablok et al. [7] proposed a high-integrity variable-position mooring system using electric and hydraulically actuated CJs to enable the chain to enter or exit to achieve the given tension or displacement. Wu et al. [8] compared CJs with six other tensioning systems in the mooring system of a deep water platform and found that the CJ is still the most popular choice for semis. Johnson et al. [9] designed a smaller semi-submersible FPSO, which uses the CJ to tighten 12 taut chain-polyester-chain mooring lines to complete the mooring of the system, eliminating the traditional mechanically complex and space-demanding winch system. The CJ-integrated push–pull hydraulic cylinder synchronously provides linear tension for mooring chains of different sizes and locates the required mooring chain segments. Compared with the windlasses and winches with the same load capacity, a CJ not only greatly reduces the space left by the deck for the mooring tensioning system but also effectively solves the problem of chain wear and excessive bending stress during the retracting process.

However, FPSO platforms operate for long periods in complex and harsh marine environments, and their mooring operations require extremely high reliability, controllability and safety from the CJs. For large and complex engineering hydraulic systems, traditional methods of predicting the exact location and magnitude of the failure within the failed part cannot be relied upon entirely. Recent advances in fault diagnosis have achieved remarkable performance through deep learning architectures. Research on fault diagnosis predominantly focuses on sensor data, employing multi-sensor fusion technology to enhance diagnostic accuracy and reliability by integrating multiple features such as vibration, temperature, pressure and flow [10–12]. Wang et al. [13] used 2D time modeling and attention mechanism fusion to decouple composite faults. Features are extracted from multi-sampling rate sensor data to achieve high-precision diagnosis of hydraulic system faults under noise conditions. Chen et al. [14] proposed a two-stage fault diagnosis method using flow data to address the issue of significant data incompleteness in hydraulic systems. Zhu et al. [15] fused vibration, pressure and acoustic sensor signals, mined the time-frequency characteristics of faults from the signals through continuous wavelet transform and used a CNN to establish an adaptive diagnosis model to identify typical faults of axial piston pumps. Xia et al. [16] simultaneously considered spatiotemporal characteristics of raw data from different sensors, avoiding manual feature extraction or selection. Gong et al. [17] directly integrated multiple sensor raw data to ensure the integrity of information for traditional diagnostic methods that rely on existing experience and manual feature extraction. However, this fusion occurs at the lowest level of information. To address the issue of diagnostic model inflexibility, Wu et al. [18] suggested a fault diagnosis model using a 1D CNN to extracts features from the vibration signal, enabling rapid end-to-end composite fault diagnosis. Building on this, Xue et al. [19] proposed a parallel multichannel structure based on a 1D CNN and 2D CNN for deep feature extraction. By using feature fusion, the method achieved more reliable fault diagnosis with fewer iterations and lower computational cost. Hao et al. [20] introduced an end-to-end solution using an LSTM network, effectively diagnosing bearing faults by fusing deep spatiotemporal features from multiple sensors. Ma et al. [21] analyzed the operating characteristics of the lifting hydraulic system of the Very Large Crude Carrier, extracted the fault sensitivity characteristics of the pressure sensor signal of the hydraulic system through WPT and classified the leakage fault based on the SVM multi-classification model. Liu et al. [22] developed a fault diagnosis method based on multi-sensor fusion, extracting spatial features using a CNN and temporal features using LSTM to identify the severity of the fault. Yang et al. [23]

established a 1D-SENets model for the fault diagnosis of axial piston pumps with a small number of training samples available. The model diagnosis and verification are carried out by the fault vibration signal of the actual working condition, and the over-fitting problem in the diagnosis process is solved. Tao et al. [24] proposed a real-time fault diagnosis method for hydraulic systems based on an MS-CNN. The model reduces the computational complexity and improves the performance of the diagnosis model by mining higher-level fault correlation features.

The sensor measurement data often contain errors, and the information obtained by different sensors can be imprecise, ambiguous, unclear or even contradictory, ultimately resulting in unreliable fusion outcomes. The concept of the attention mechanism was first proposed by cognitive neuroscientists who conducted research in this field [25]. The model employs a weighting system that assigns varying degrees of importance to different input components, thereby facilitating the extraction of crucial information while simultaneously reducing the computational and storage overhead associated with the model [26]. The attention mechanism is integrated into the DNN structure, enabling its learning alongside other network parameters [27]. Wang et al. [28] introduced an attention mechanism module to enhance fault-related feature learning, combining it with a 1D CNN to adaptively recalibrate features at each level, significantly improving discriminative feature representation. Shao et al. [29] developed an autonomous ship navigation model using multiple sensors to obtain state information. They enhanced the modelling capability by extending the deformable convolution and introducing a self-designed attention mechanism. Wu et al. [30] proposed an IES short-term load forecasting method based on an attention-based CNN combined with LSTM and BiLSTM models. Gao [31] proposed a detection method that integrates a CNN and BiLSTM network, where the CNN captures local features, and BiLSTM extracts long-range dependencies. An attention mechanism is incorporated to enhance classification accuracy. Long et al. [32] developed an improved AdaBoost-based motor fault diagnosis method utilizing an attention mechanism and multi-sensor data.

As can be seen from the above, although many scholars have conducted in-depth research on the fault diagnosis technology of the hydraulic system, the real-time fault diagnosis technology of the hydraulic system of the CJ has not been widely studied. The CJ equipment developed in this paper has a strong coupling effect and high nonlinearity. The hydraulic lifting cylinder is the main actuator, cooperating with the clamping and limiting hydraulic cylinder group. Due to the interference of actual complex sea conditions, the failure rate is significantly higher than that of land-based equipment, and the fault is difficult to detect. Especially under diverse operating conditions, the sensitivity to different degrees of fault characteristics is different, and the early fault of a low load is very difficult to be detected in time. In order to adaptively perform real-time fault diagnosis of the CJ under complex loads, this study proposes a deep neural network model based on a GAM, which enhances the ability of a model to capture the previous and subsequent information. The model ensures robustness across diverse load conditions while identifying key sensor features to optimize sensor layout. The innovations of this study are as follows:

1. This study investigated typical fault mechanisms in CJ operations under varying loads and designed a CNN-BiLSTM-GAM hierarchical model.
2. The model integrates multi-scale local and global features, capturing fault patterns in short intervals and persistent behaviors across time scales, ensuring accurate and robust fault diagnosis under dynamic load conditions.
3. A multi-scale GAM dynamically adjusts feature importance across time steps and sensors, enabling key sensor selection and layout optimization.

2. Methods and Models

During the operation of the CJ, fault occurrences can lead to significant variations in critical physical parameters. The CJ system prototype developed in this study accurately replicates the dynamic characteristics and functional properties of an actual spread mooring system. Through the design of a non-destructive fault injection test platform, various typical fault conditions were precisely simulated. To address the uncertainty in time-series signals caused by sensor measurement errors, the research team deployed a pressure sensor array (FS1–FS11), temperature sensor network (TS1–TS12) and flow monitoring units (FS1–FS5) at key nodes of the hydraulic actuators, establishing a synchronized multi-physical quantity acquisition system. However, while this distributed sensor network enhances system observability, it inevitably introduces challenges, such as increased computational complexity and sensor data conflicts. Hence, this paper innovatively proposes a deep network diagnostic framework based on a GAM. The proposed model achieves precise identification of faults with varying severity, including internal pump leakage (I0–I2), proportional solenoid valve conditions (V0–V3) and circuit pipe blockages (P0–P3). By incorporating the GAM, the model not only accomplishes accurate fault classification but also generates a sensor importance evaluation matrix, providing quantitative guidance for optimizing the configuration of the sensor network.

2.1. CNN-GAM Model Architecture

This paper discusses the application of the CNN-GAM and CNN-BiLSTM-GAM model in fault diagnosis and sensor optimization. The model is trained and validated by fusing multi-scale time-series data with different fault severities under full-load conditions. The performance of the model is tested under half-load conditions.

Initially, this study employs a CNN integrated with a GAM to assess the severity of hydraulic system faults under varying load conditions, as illustrated in Figure 1. The convolutional layer extracts spatial local features from the multivariate time-series data, which are then weighted by the GAM to emphasize the most critical features and evaluate each sensor's importance.

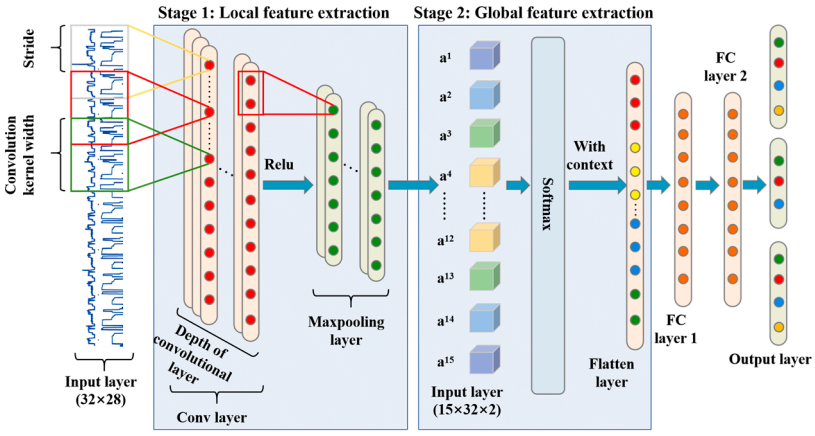


Figure 1. The architecture of the CNN-GAM fault diagnosis model.

The primary function of CNNs in fault identification is to extract local features from input data via convolution operations. For sensor or time-series data, local features often reveal critical patterns or anomalies within the signal, providing valuable insights into system behavior. By utilizing convolutional layers, the model can automatically learn these features, enhancing its ability to comprehend local data structures and facilitating the detection of potential fault signals. The data from 28 multivariate sensors are input into a 1D convolutional layer with a batch size of 32, allowing for hierarchical feature

extraction through stacked convolutional layers. The ReLU activation function is employed to mitigate the issue of gradient disappearance. Following each convolutional layer, a max pooling layer performs sampling aggregation to complete local feature extraction. The output of the convolutional network serves as input for the self-attention mechanism. The CrossEntropy loss function iteratively updates weights using the error backpropagation algorithm, facilitating the optimal convergence of the loss function. A fully connected (FC) layer calculates the weight of each feature, acting as a classifier where its input is the convolutional layer output, and its output represents the feature weights. By multiplying these weights with the convolutional output, we obtain the weighted features, which are then passed to the FC layer to generate the final classification result using the Softmax activation function. The Adam optimizer is employed during training with a learning rate of 0.001, and the model undergoes training for 50 epochs. In each epoch, the training set undergoes forward and backward propagation to update the weights, using a mini-batch gradient descent strategy with a batch size of 32. After each epoch, hyperparameter tuning is performed on the validation set to evaluate model performance and select the optimal configuration.

This approach optimizes sensor placement, reducing the model's computational costs while accurately identifying fault severity. Assume that $\mathbf{P} = \{p_1, p_2, \cdots, p_{11}\}$, $\mathbf{F} = \{f_1, f_2, \cdots, f_5\}$ and $\mathbf{T} = \{t_1, t_2, \cdots, t_{12}\}$ represent the input data from the 11 pressure sensors, 5 flow sensors and 12 temperature sensors, respectively. The input of the model can be expressed as follows:

$$\mathbf{X} = [\mathbf{P}, \mathbf{F}, \mathbf{T}] \in \mathbb{R}^{N \times T \times d_p} \tag{1}$$

The CNN layer extracts local spatial features from multivariate time-series data. Convolutional filters use a sliding window to scan the data, highlighting critical fault-related features in short time intervals. Equation (2) demonstrates how the CNN extracts local features at different scales.

$$\mathbf{H}_s = \mathrm{ReLU}(\mathrm{Conv1D}(\mathbf{X}, \mathbf{W}_s) + \mathbf{b}_s) \tag{2}$$

where $s = 1, 2, \cdots, S$, S represent the number of convolutional kernels at different scales; $\mathbf{W}_s$ denotes the weights of the convolutional kernel at the s-th scale; and b_s is the bias term. The GAM dynamically assigns weights to different features through weighted summation, enabling the selection and fusion of features extracted by the CNN while suppressing redundant and irrelevant features.

2.2. CNN-BiLSTM-GAM Model Architecture

While the CNN-GAM fault diagnosis model effectively extracts fine-grained features through local convolution and captures global features via the attention mechanism, its performance may be suboptimal under actual operating conditions. This decline arises from the dynamic progression of hydraulic system fault severity over time, where critical fault information may be obscured by long-term dependencies in the time-series data, ultimately reducing diagnostic accuracy. Hence, this paper proposes an innovative CNN-BiLSTM-GAM hybrid architecture based on the fusion of multi-scale time-series data features under variable load conditions, as illustrated in Figure 2.

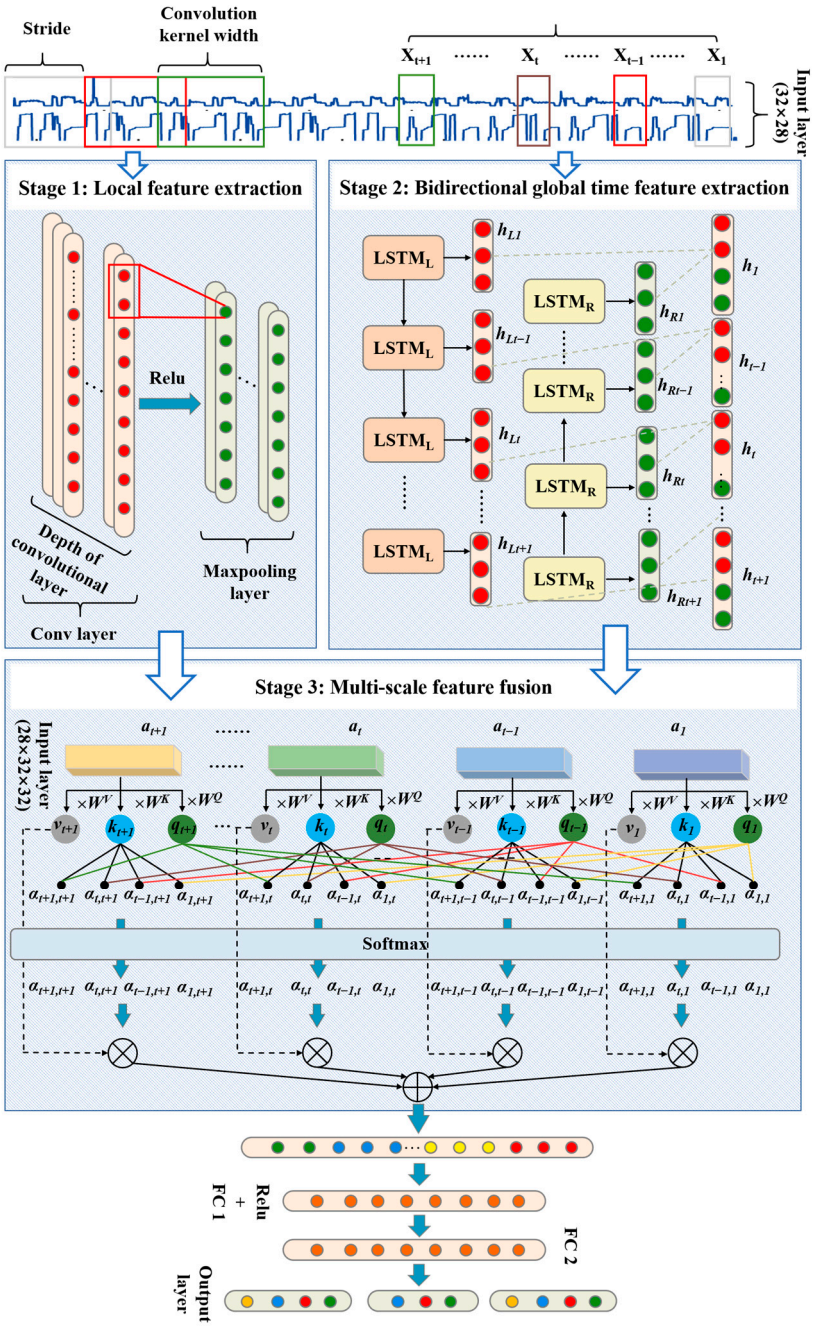


Figure 2. The architecture of the CNN-BiLSTM-GAM fault diagnosis model.

The proposed model establishes a hierarchical feature learning framework that synergistically integrates the spatial pattern recognition capability of a CNN with the temporal dynamics modeling strength of BiLSTM, further enhanced by a GAM. The CNN component extracts spatial features for preliminary fault type identification, while the BiLSTM network precisely captures the grained evolution of fault severity from initial stages to complete failure, thereby enabling early fault detection essential for predictive maintenance. This addresses the limitations of conventional CNN-BiLSTM networks in preserving subtle fault signatures, particularly under half-load conditions where fault characteristics become significantly attenuated. The core innovation of this research lies in the implementation of the GAM as an intelligent feature regulator that performs 3D attention weighting. Firstly, the spatial-dimension weighting across sensor channels emphasizes critical measurement points while simultaneously filtering redundant sensors through weight screening, thereby reducing computational overhead. Secondly, temporal-dimension weighting along the time

series reinforces key fault progression patterns, providing crucial support for the real-time condition monitoring of CJ systems. Finally, cross-layer hierarchical weighting preserves diagnostically relevant yet weak features during feature fusion, enhancing the model's adaptability across diverse operating conditions. This multi-scale attention mechanism dynamically recalibrates feature importance at different abstraction levels, effectively overcoming the signal-to-noise ratio challenge in half-load fault detection while maintaining high sensitivity to incipient fault symptoms. The proposed architecture demonstrates exceptional performance in characterizing the nonlinear interactions between load variations and fault progression characteristics, establishing a new benchmark for condition monitoring in hydraulic systems. The methodology advances the field by providing a robust framework for early fault identification and system health management under complex operational scenarios.

The proposed CNN-BiLSTM-GAM model employs carefully configured parameters to optimize its temporal modeling and attention mechanisms. For the BiLSTM component, we set the hidden dimension to 16 units with a single recurrent layer, adopting a bidirectional configuration to capture both forward and backward temporal dependencies in the hydraulic system data. This compact yet effective design yields a total of 2112 trainable parameters for the BiLSTM layer, balancing model complexity with computational efficiency. The GAM is implemented with 2 parallel attention heads operating on the 32-dimensional feature space. This configuration creates multiple representation subspaces that jointly attend to different temporal patterns in the fault evolution process. The attention layer introduces 4160 parameters. The CrossEntropy loss function is chosen to suit the multi-category classification task. During model training, the Adam optimization algorithm is utilized with a learning rate of 0.001, enabling efficient parameter updates and promoting rapid convergence. A batch size of 32 is selected to balance memory stability and model learning efficiency. The model undergoes 50 training cycles to capture the underlying data patterns adequately. The BiLSTM output at each scale can be expressed as follows:

$$\begin{gathered} \overrightarrow{\mathbf{h}}_{t,s} = \mathrm{LSTM}_{\mathrm{fwd}}(\mathbf{H}_s, t), \quad \overleftarrow{\mathbf{h}}_{t,s} = \mathrm{LSTM}_{\mathrm{bwd}}(\mathbf{H}_s, t), \\ \mathbf{H}_{b,s} = \left[\overrightarrow{\mathbf{h}}_{t,s}; \overleftarrow{\mathbf{h}}_{t,s}\right] \in \mathbb{R}^{N \times T \times d_p} \end{gathered} \tag{3}$$

where $\overrightarrow{\mathbf{h}}_{t,s}$ and $\overleftarrow{\mathbf{h}}_{t,s}$ represent the time-dependent features extracted at each scale s; $\mathbf{H}_{b,s}$ denotes the concatenated features from the forward and backward directions.

The GAM is used to fuse features from different time steps, sensors and scales, dynamically adjusting the importance of these features. Through the GAM, the model assigns different attention weights based on the contribution of each sensor and time point to fault severity. The multi-scale properties enable the model to focus on faults occurring at various time scales, ensuring it captures both immediate fault behaviors and persistent fault patterns. The features after global fusion are shown in Equation (4).

$$\begin{gathered} \mathbf{A}_s = \mathrm{Softmax}\left(\frac{\mathbf{Q}_s \mathbf{K}_s}{\sqrt{d_k}}\right), \quad \mathbf{A} = \sum_{s=1}^{S} \gamma_s \cdot \mathbf{A}_s \\ \mathbf{H}_g = \mathbf{A} \cdot \left(\sum_{s=1}^{S} \gamma_s \cdot \mathbf{V}_s\right) \end{gathered} \tag{4}$$

where $\mathbf{Q}_s$, $\mathbf{K}_s$ and $\mathbf{V}_s$ represent the features generated by the GAM layer; $\mathbf{A}_s$ is the attention matrix across time steps; and γ_s and $\mathbf{A}_s$ represent the weights at the s-th scale and the attention weights from multi-scale fusion, respectively.

By integrating an importance weight mechanism, the overall architecture enables the model to adapt effectively to multi-dimensional features, improving robustness and classi-

fication accuracy for complex data. The final global features are computed by dynamically weighting the sensors and time steps, as shown in Equation (5).

$$\mathbf{H}_{\text{final}} = \sum_{t=1}^{T} \alpha_t \cdot \sum_{j=1}^{d_p} \beta_j \cdot \mathbf{H}_g(t, j) \tag{5}$$

where α_t and β_j denote the weights of the t-th time step and the j-th sensor dimension, respectively.

Following feature extraction, classification is performed using the fully connected (FC) layer. The FC1 layer utilizes batch normalization to expedite the training process and improve the stability of the model. The final output layer maps the extracted features to identify varying degrees of the three fault types, as shown in Equation (6). This structural design maximizes the potential information within time-series data, offering an effective solution for fault diagnosis tasks.

$$y = \text{softmax}(\mathbf{W}_o \mathbf{H}_{\text{final}} + \mathbf{b}_o) \tag{6}$$

3. Experimental Work

The hydraulic fault simulation test bench presented in this study is a sophisticated, multi-functional testing device that can be categorized into two primary components. The first component is the hydraulic mechanical structure, which encompasses the limit, clamping and lifting systems. The second component consists of the measurement and control system, including an upper computer (PC), a lower computer (PLC) and sensors for gathering the system's physical parameters. These elements collaborate effectively to achieve automated control of fault simulation tests and ensure precise collection of system parameters.

3.1. Experimental Bench

The principle and function of the CJ prototype of the test bench are the same as those of the actual spread mooring system. It mainly uses the lifting hydraulic cylinder group to realize the segmented lifting of the loaded anchor chain, and uses the limit and clamping hydraulic cylinder group to realize the limit and clamping of the load anchor chain, so as to prevent the chain from slipping under load. The main structure and physical diagram of the prototype of the hydraulic fault simulation test bench for the CJ are shown in Figure 3.

The test bench realizes the segmented retracting and releasing of the loaded chain under the cooperation of lifting, clamping and limiting hydraulic cylinder groups. To lift the chain, the piston of the cylinder group extends outward, releasing the clamp's restriction on the chain. As the pivot of the clamping cylinder group moves inward, the chain link is clamped by the clamping clamp. The lifting hydraulic cylinder group promotes the lifting beam to move upward. A piston moves inward when it moves to the top dead center to reach the stroke limit of the lifting hydraulic cylinder group. Limiting clamps restrict chain links, clamping hydraulic cylinders move outward and clamping clamps release the clamping effect on chain links. At this time, the lifting hydraulic cylinder group drives its own mechanism to move downward to the stroke limit of the bottom dead center. The test bench repeats the above working cycle, and the chain is lifted in sections to raise the load to the working position. The need to reset the chain operation and the lifting of the loaded chain step is opposite.

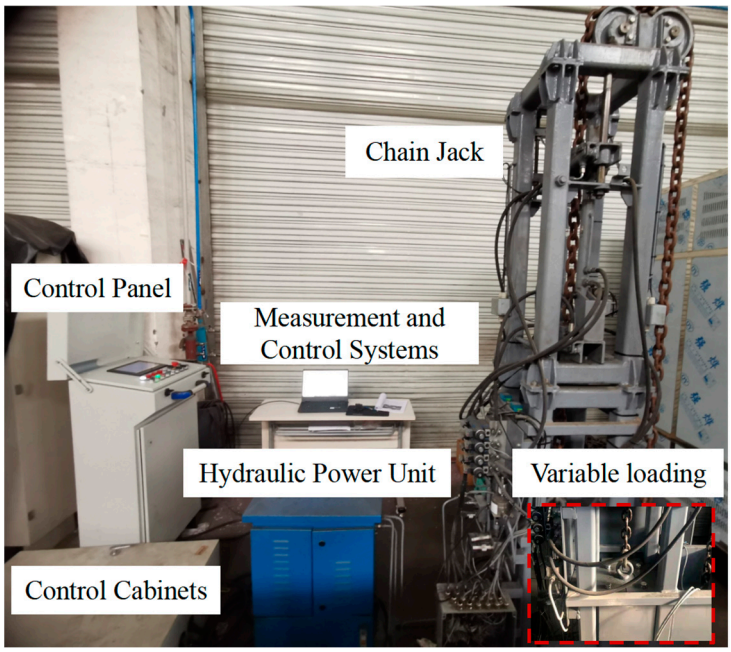


Figure 3. Composition of chain jack hydraulic system test bench.

3.2. Experimental Description

Based on the working principle of the CJ, the hydraulic system of the test bench comprises three subsystems: the hydraulic clamping system (HCS), hydraulic lifting actuator (HLA) and hydraulic limiting system (HLS). The HLS controls the hydraulic cylinder group to restrict the mooring chain. Firstly, the HCS controls the opening and closing of the mooring chain clamping mechanism for chain clamping. Subsequently, the HLA is used to deploy and retrieve the chain for mooring tension regulation. Finally, the limit clamp mechanism is driven by HLS to constrain the position of the mooring chain to prevent the chain from falling off. The three subsystems cooperate with each other to complete the work cycle under the same hydraulic tank and hydraulic pump drive. The fault injection principle and sensor arrangement of the CJ hydraulic system simulation are shown in Figure 4.

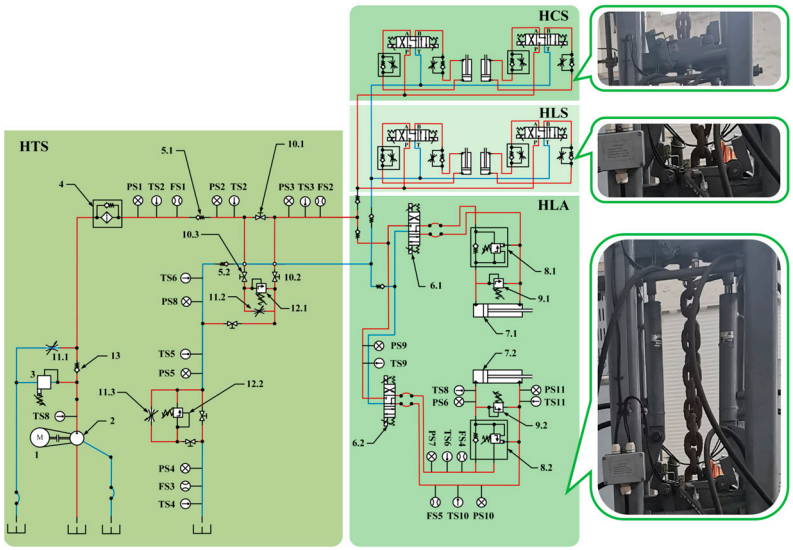


Figure 4. Fault injection principle and sensor layout diagram of CJ hydraulic system.

Through the normal operation of the lifting system, the analog fault injection module controls the adjustable throttle valves 11.1, 11.2 and 11.3 to be closed. The motor 1 drives the hydraulic pump 2 to work and output the pressure oil, which is transmitted to the high-pressure filter 4, the check valve 5.1, the ball valve 10.1, the electromagnetic directional valves 6.1 and 6.2 and the hydraulic cylinder group 7, and then changes the flow direction through the electromagnetic directional valve group, flows through the check valve 5.2, the ball valve 10.6 and finally flows back to the oil tank to complete a working cycle.

The hydraulic fault simulation test bench of the CJ allows for reversible changes in each component to achieve fault simulation injection. The hydraulic system may have multiple faults at the same time, and the duration, severity and type of faults are different. Non-destructive simulation fault injections were conducted using the lifting hydraulic system of the test bench. By adjusting the switches of the relevant valve components and coordinating their settings, specific simulation fault injections were designed for three hydraulic system components: the power component (hydraulic pump leakage), the executive component (proportional solenoid valve conditions) and the control component (circuit pipe blockage). The methods for simulating different fault types are as follows:

Circuit pipe blockages: Check valve 5.1 as a simulation of the blockage object. In the lifting system work, in turn, open the hydraulic circuit of the ball valve 10.2, adjustable throttle valve 11.2 and the ball valve 10.3 and then close the ball valve 10.1, by adjusting the opening of the throttle valve 11.2 to simulate the different levels of blockage of the check valve. The safety valve 12.1 plays a role in overload protection.

Internal pump leakage: The leakage of hydraulic pump 2 is realized by connecting an adjustable throttle valve 11.1 in series between the outlet of the hydraulic pump and the fuel tank. The different leakage levels of the hydraulic pump are simulated by adjusting the opening of the throttle valve. In order to prevent the backflow of hydraulic oil during the leakage test of the simulated hydraulic pump, a check valve 13 is installed at the outlet of the hydraulic pump to ensure the flow direction of the oil circuit.

Proportional solenoid valve conditions: The proportional solenoid reversing valve is a hydraulic control component that plays a conversion role between the hydraulic control system and the electrical control system. It can not only change the direction of the hydraulic oil flow but also control the reversing speed and flow. Valve spool stagnation can cause improper operation, leading to abnormal pressure and flow fluctuations before and after the proportional solenoid directional valve in the hydraulic system. By manually adjusting the current settings of proportional solenoid directional valves 6.1 and 6.2 via the PLC control panel, different spool movements are controlled, altering the flow rate through the directional valve to simulate varying degrees of spool stall.

3.3. Data Acquisition

Developing a fully operational hydraulic failure simulation test bench necessitates the integration of a robust measurement and control system. This system must precisely regulate hydraulic actuators, execute specified action functions and evaluate system parameters under diverse environmental conditions. In this study, the measurement and control system for the CJ hydraulic failure simulation test bench employs a programmable logic controller (PLC) for the lower computer, utilizes a C++ environment for the upper computer software and establishes communication between the two systems via the Modbus-TCP protocol to facilitate data interaction and control.

To fulfil data acquisition requirements, the measurement and control system of the test bench must encompass the following functionalities:

1. The sensors used in the test bench should have a fast frequency response, which can accurately and sensitively collect physical quantities. The test bench allows for

simultaneous sampling of the pressure, flow rate and temperature sensors at varying rates, with the maximum sampling frequency exceeding 100 Hz. At the same time, the sampling rate of each sensor is self-adjustable, and the collected analogue quantity is delayed in the PLC after processing. After processing, it is displayed and stored on the PC.

2. The PC manages and adjusts the test parameters, while operators can manually configure the console and touch screen on the lower-level PLC. The control program supports adjustments to accommodate varying test requirements, including different load conditions, simulated fault types and fault severity.
3. In addition to the inherent sampling channels of the test bench, additional channels are reserved to accommodate future needs. Both the lower-level PLC and upper-level control software are designed using a modular architecture, enabling flexible modifications and facilitating the secondary development of the test bench.
4. The test bench console and touch screen are configured with select switches, function buttons, operation indicator lights, etc. The lower-level PLC is responsible for managing the input and output states of both analog and digital signals, ensuring precise control and data acquisition. When the test is abnormal, the relevant indicator lights will issue an early warning signal.
5. It ensures seamless communication and interactive control between devices by providing the required network and USB interfaces.
6. Equipped with a UPS power failure protection function, the system prevents test data loss in the event of an accidental power outage.

According to the principles of fault simulation and injection, three fault types are simulated under variable load conditions in the lifting hydraulic system: internal pump leakage, circuit pipe blockage and proportional solenoid valve conditions. To comprehensively simulate various fault scenarios, different severities are defined for each fault condition. The physical parameters of the hydraulic system under diverse operating conditions are collected, yielding a substantial dataset for subsequent fault diagnosis research. Notably, the varying severity of each fault requires threshold adjustments, which can be performed either manually or automatically. To maintain system safety, these thresholds must be meticulously calibrated based on comprehensive testing and debugging. The prior study [22] outlines the detailed analysis process. As shown in Figure 5, FS2 is used as an example to analyze the real-time data of multivariate time series with severities of fault under variable load conditions. Figure 5a presents the real-time dataset for circuit pipe blockage severity under varying load conditions, categorized into four levels: no blockage (P0), weak blockage (P1), severe blockage (P2) and close to total failure (P3). Figure 5b illustrates the dataset for internal pump leakage severity, classified into three levels: no leakage (I0), weak leakage (I1) and severe leakage (I2). Figure 5c displays the dataset for valve condition faults, also under different load conditions, divided into four levels: optimal switching behavior (V0), small lag (V1), severe lag (V2) and close to total failure (V3).

This paper employs a deep neural network architecture based on a self-attention mechanism to diagnose and identify varying degrees of three fault types. The fault time-series data collected in Section 3 serve as inputs to the network, with 80% of the samples under full load utilized as the training dataset and 10% reserved for model validation. Given that the hydraulic system experiences variable loads during actual operations, data samples from 10% half-load conditions are further used as test datasets to evaluate the model's diagnostic performance across different load scenarios, as illustrated in Table 1.

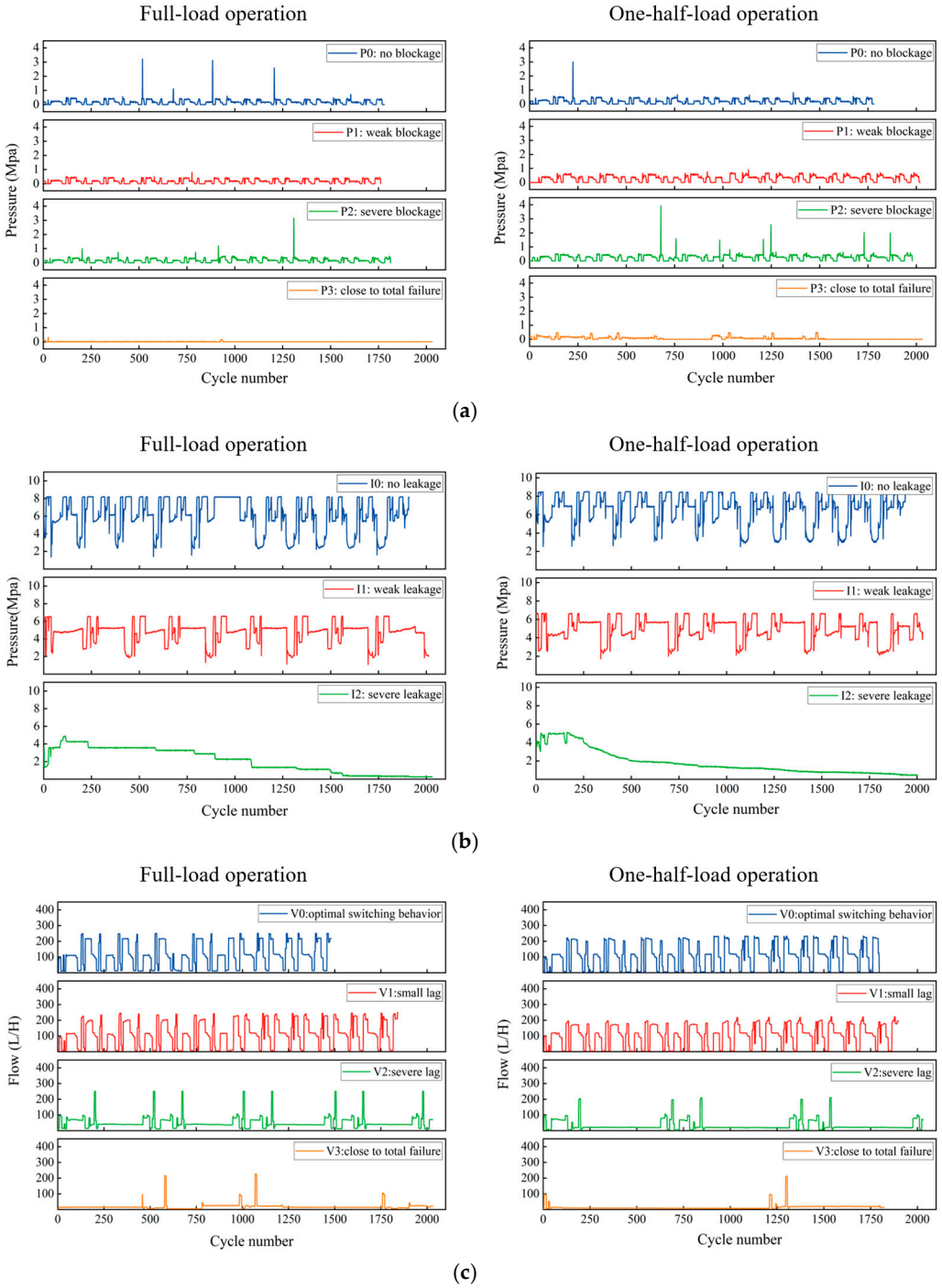


Figure 5. Sensor data of different severity faults under variable load operation: (**a**) circuit pipe blockage; (**b**) internal pump leakage; and (**c**) valve condition.

Table 1. Dataset statistics used for model construction.

Classification	Original	Training	Validation	Test
Circuit pipe blockage	29,940	23,952	2994	2994
Internal pump leakage	35,430	28,344	3543	3543
Valve condition	31,500	25,200	3150	3150
Total	**96,870**	**77,496**	**9687**	**9687**

4. Results and Discussion

4.1. Comparison of Different Models on Full-Load Operation

In this study, the CNN-GAM fault diagnosis model was developed to address varying severities of faults. The pre-processed training dataset is used as input, and the CNN is used to extract local spatiotemporal features from different sensors to capture the spatial correlation between sensors. Subsequently, the GAM is introduced to dynamically weight different time points and sensor features to capture global dependencies and features. Ultimately, the model weights corresponding to the highest validation set accuracy are preserved for subsequent analysis and testing. Figure 6 shows the accuracy curve and loss curve of the CNN-GAM model. Figure 6a shows the rapid increase and fluctuation of the accuracy curve in the initial stage, reflecting its instability in the convergence process. Although it gradually stabilizes, this fluctuation will affect the final diagnostic performance. The overall accuracy of the model is only 91.98%. This shows that the model can capture data features well in the early stage, but its learning ability is limited in the subsequent training. Figure 6b is the loss curve. In the initial training phase, the loss associated with circuit pipe blockage and proportional solenoid valve conditions decreased rapidly. However, the loss related to internal pump leakage began to decline only after epoch 10. This indicates that the model struggled to fully capture complex features when processing the multivariate time-series data from multiple sensors.

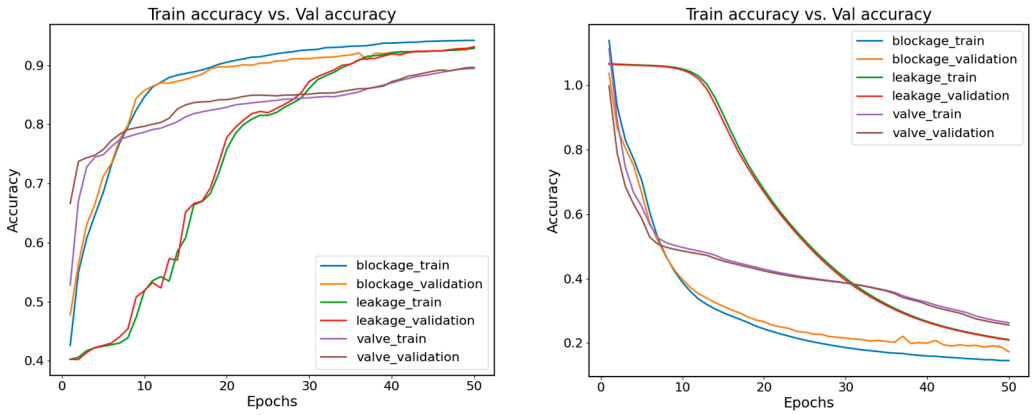
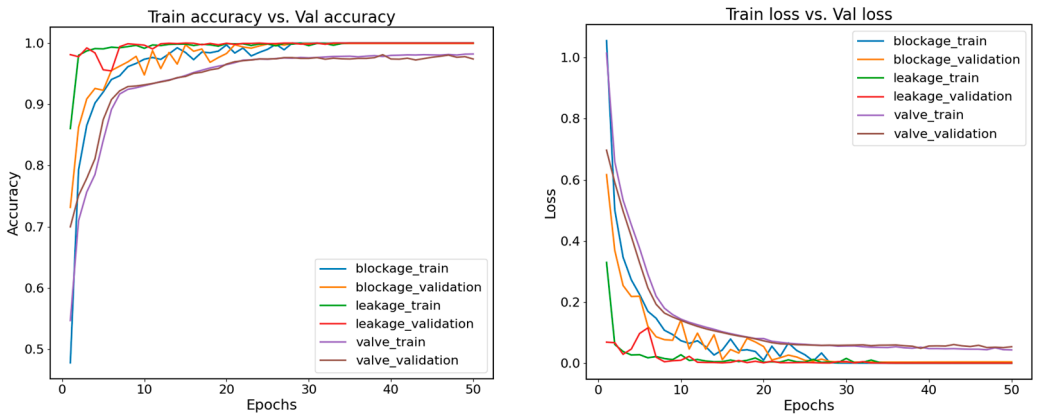


Figure 6. Performance of the CNN-GAM model: (**a**) accuracy curves; (**b**) loss curves.

Consequently, the CNN-BiLSTM-GAM fault diagnosis model is proposed. The early stopping strategy is applied to monitor performance on the test set, ensuring robust generalization of the model. Figure 7 presents the accuracy and loss curves of the CNN-BiLSTM-GAM model. In Figure 7a, the accuracy curve indicates a consistent upward trend, achieving 100% diagnostic accuracy for varying degrees of blockage and internal pump leakage and 98.10% for valve conditions. The overall diagnostic model exhibits an impressive accuracy of 99.34%, highlighting its effectiveness in processing multivariate time-series data. Figure 7b displays the loss curve of the CNN-BiLSTM-GAM model, which shows a smooth decline, particularly in the later training stages, indicating strong convergence performance. These results demonstrate that the CNN-BiLSTM-GAM model possesses enhanced robustness and effectiveness in fault diagnosis tasks, allowing it to accommodate complex data features better.



(**a**) (**b**)

Figure 7. Diagnostic results of the CNN-BiLSTM-GAM model: (**a**) accuracy curves; (**b**) loss curves.

The specific diagnostic result comparison indicators of the CNN-GAM model and CNN-BiLSTM-GAM model are shown in Table 2. The CNN-BiLSTM-GAM model was tested on 2994 circuit pipe blockage samples, 3543 internal pump leakage samples and 3150 proportional solenoid valve condition samples. The CNN-BiLSTM-GAM model has a diagnostic accuracy of up to 99.34% for different severities and has reached 100% in fault diagnosis for internal pump leakage. Therefore, this study used the CNN-BiLSTM-GAM model to perform multi-fault diagnosis on the hydraulic system of the CJ under different load conditions.

Table 2. Comparison metrics for models.

Models	Classes	Severity	Precision	Recall	F1-Score	Support
CNN-GAM	Circuit pipe blockage	P0	83.79%	96.54%	89.72%	723
		P1	99.14%	94.01%	96.51%	735
		P2	92.95%	84.59%	88.57%	811
		P3	98.62%	98.76	98.69%	725
		Macro avg	93.63%	93.48%	93.37%	2994
		Accuracy		93.22%		
	Internal pump leakage	I0	96.37%	90.55%	93.37%	762
		I1	90.61%	92.33%	91.46%	1421
		I2	93.98%	95.29%	94.63%	1360
		Macro avg	93.65%	92.72%	93.15%	3543
		Accuracy		93.08%		
	Valve condition	V0	94.01%	93.01%	93.51%	844
		V1	89.93%	94.23%	92.03%	919
		V2	90.03%	84.90%	87.39%	755
		V3	83.13%	84.18%	83.65%	632
		Macro avg	89.27%	89.08%	89.14%	3150
		Accuracy		89.65%		
	Diagnostic accuracy			**91.98%**		

Table 2. *Cont.*

Models	Classes	Severity	Precision	Recall	F1-Score	Support
CNN-BiLSTM-GAM	Circuit pipe blockage	P0	99.86%	100%	99.93%	723
		P1	100%	100%	100%	735
		P2	100%	99.75%	99.88%	811
		P3	99.86%	100%	99.93%	725
		Macro avg	99.93%	99.94%	99.93%	2994
		Accuracy		99.93%		
	Internal pump leakage	I0	100%	100%	100%	762
		I1	100%	100%	100%	1421
		I2	100%	100%	100%	1360
		Macro avg	100%	100%	100%	3543
		Accuracy		100%		
	Valve condition	V0	100%	99.29%	99.64%	844
		V1	96.67%	97.82%	97.24%	919
		V2	99.60%	99.60%	99.60%	755
		V3	95.85%	95.09%	95.47%	632
		Macro avg	98.03%	97.95%	97.99%	3150
		Accuracy		98.10%		
	Diagnostic accuracy			**99.34%**		

4.2. Discussion on the Results of CNN-BiLSTM-GAM Model on Half-Load Conditions

The test bench designed and developed in this paper is equipped with redundant sensors at the same position, including 11 pressure sensors (PS1–PS11), 12 temperature sensors (TS1–TS12) and 5 flow sensors (FS1–FS5). However, this approach inevitably leads to a substantial increase in computational cost during the training of the fault diagnosis model. Therefore, when building a deep network fault diagnosis model based on the self-attention mechanism, this paper introduces trainable importance weights, enhances the flexibility of feature selection and calculates the contribution of each sensor in the diagnosis process. Combined with the sensor layout of the test bench, the high weight is selected from the redundant sensors. While reducing the calculation cost, the accurate condition monitoring of the CJ is ensured. Figure 8 shows the sensor weight statistics of the CNN-BiLSTM-GAM model of training and verification. Specifically, Figure 8b–d illustrates the sensitivity of sensors to different fault types by quantifying their contribution weights through the GAM mechanism, thereby demonstrating the interpretable weight allocation in the diagnostic process. The analysis reveals distinct sensor response patterns: during pipe blockage, the influence of sensor sequential data follows the hierarchy of TS > PS > FS. Conversely, for internal pump leakage and valve condition, PS and FS exhibit predominant diagnostic importance. These findings provide empirical validation of the GAM module's capability to dynamically prioritize sensor inputs based on fault-specific characteristics. The final sensor importance distribution, obtained through averaged normalization of individual sensor weights, is presented in Figure 8a as the model's overall sensor weight statistics. Based on the actual layout of the system, pressure sensors (PS1, PS3, PS4, PS8, PS10 and PS11), temperature sensors (TS3, TS4, TS5, TS10 and TS11) and flow sensors (FS2, FS3 and FS4) were selected as inputs for the test model.

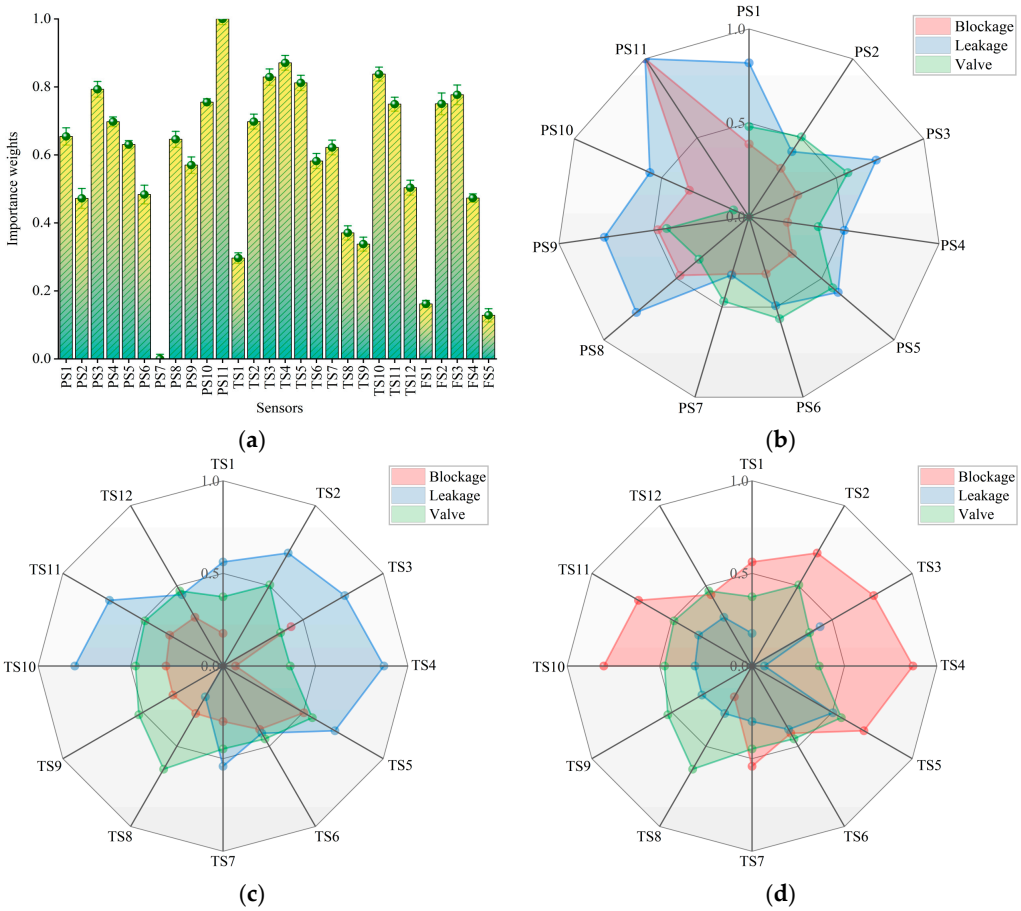


Figure 8. Sensor importance weight assignment of CNN-BiLSTM-GAM model: (**a**) overall weights; (**b**) pressure sensors; (**c**) temperature sensors; and (**d**) flow sensors.

To further test the generalization ability of the model, 14 high-importance sensors were selected based on the previous analysis. Multivariate time-series data under half-load conditions were employed as the test set to evaluate the diagnostic performance across different severities. Figure 9 illustrates the diagnostic results of the CNN-BiLSTM-GAM in identifying the various severities of each fault under half-load conditions. Figure 9a demonstrates the classification performance for circuit pipe blockage faults across five severity levels (P0–P4). The model exhibits perfect diagnostic accuracy (100%) for all severity grades, with the exception of a negligible 0.12% misclassification rate where P2 is erroneously identified as P3. Figure 9b illustrates the recognition results for internal pump leakage levels (I0–I2). The model achieves 100% recognition accuracy for all severity grades. Figure 9c presents the recognition results for proportional solenoid valve conditions (V0–V3). The identification reveals that a portion of samples are misclassified as V3: specifically, 0.36% of the V0 samples, 2.18% of the V1 samples and 0.4% of the V2 samples. Additionally, 4.91% of the V3 samples are misclassified as V1, and 0.36% of the V0 samples are misclassified as V2. In summary, the CNN-BiLSTM-GAM diagnosis model effectively determines fault severity by analyzing multivariate time-series data.

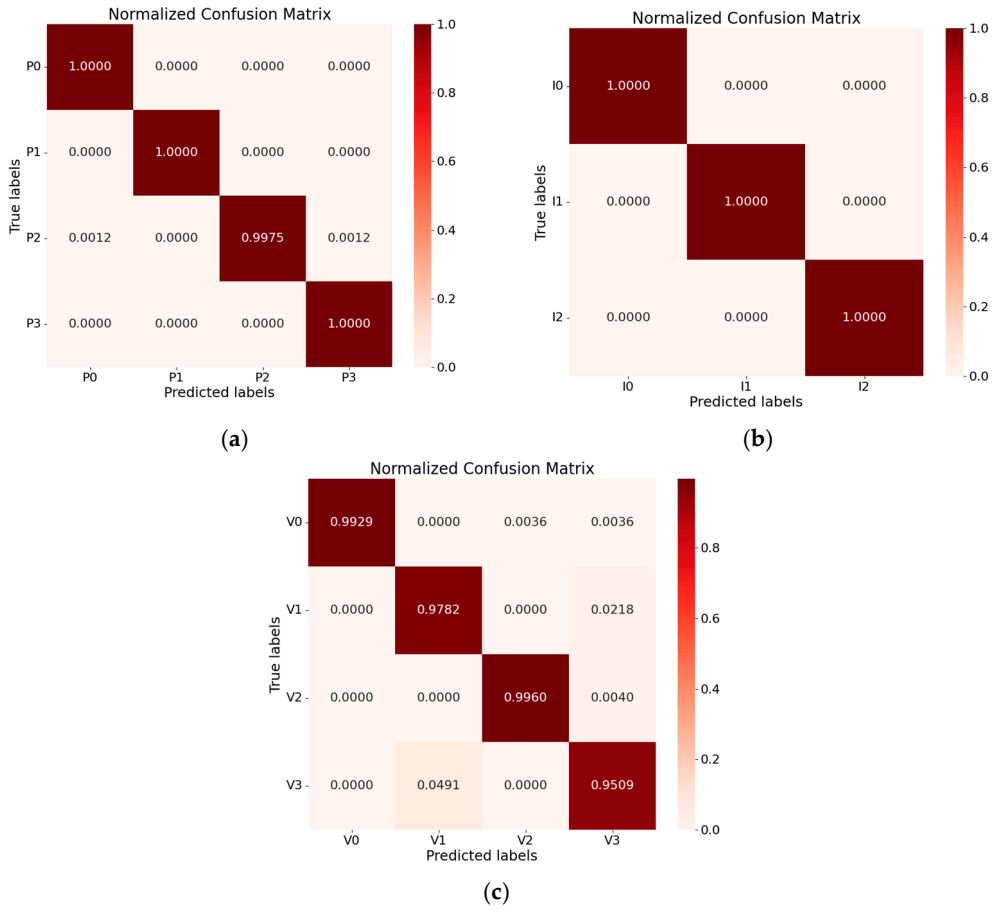


Figure 9. Confusion matrix of fault severities under test data: (**a**) circuit pipe blockage; (**b**) internal pump leakage; and (**c**) valve condition.

Specifically, t-SNE is employed to project the high-dimensional features of each layer into a two-dimensional space, highlighting the clustering of different fault categories within the feature space and guiding the optimization of the model's structure and parameters. Figure 10 illustrates the data feature distribution of the CNN-BiLSTM-GAM model, showcasing layer-by-layer learning across varying fault severities. In Figure 10a, the data features exhibit a disordered distribution from the CNN layer output; in Figure 10b, the data features exhibit a disordered distribution from the BiLSTM layer output; Figure 10c displays the feature distribution after learning through the GAM layer, demonstrating an improved aggregation of faults; and Figure 10d presents the output visualization of the FC1 layer, which effectively clusters faults, indicating that the CNN-BiLSTM-GAM model struggles to extract meaningful features from the original time-domain signal.

The receiver operating characteristic (ROC) curve and the area under the curve (AUC) are critical metrics for evaluating the performance of supervised classification models. The ROC curve illustrates the relationship between sensitivity and specificity, with sensitivity and specificity calculated at various threshold points of continuous variables. The ROC curve plots the true positive rate (TPR) against the false positive rate (FPR), with sensitivity on the vertical axis and specificity on the horizontal axis. This curve is generated by calculating sensitivity and specificity at various threshold points of continuous variables.

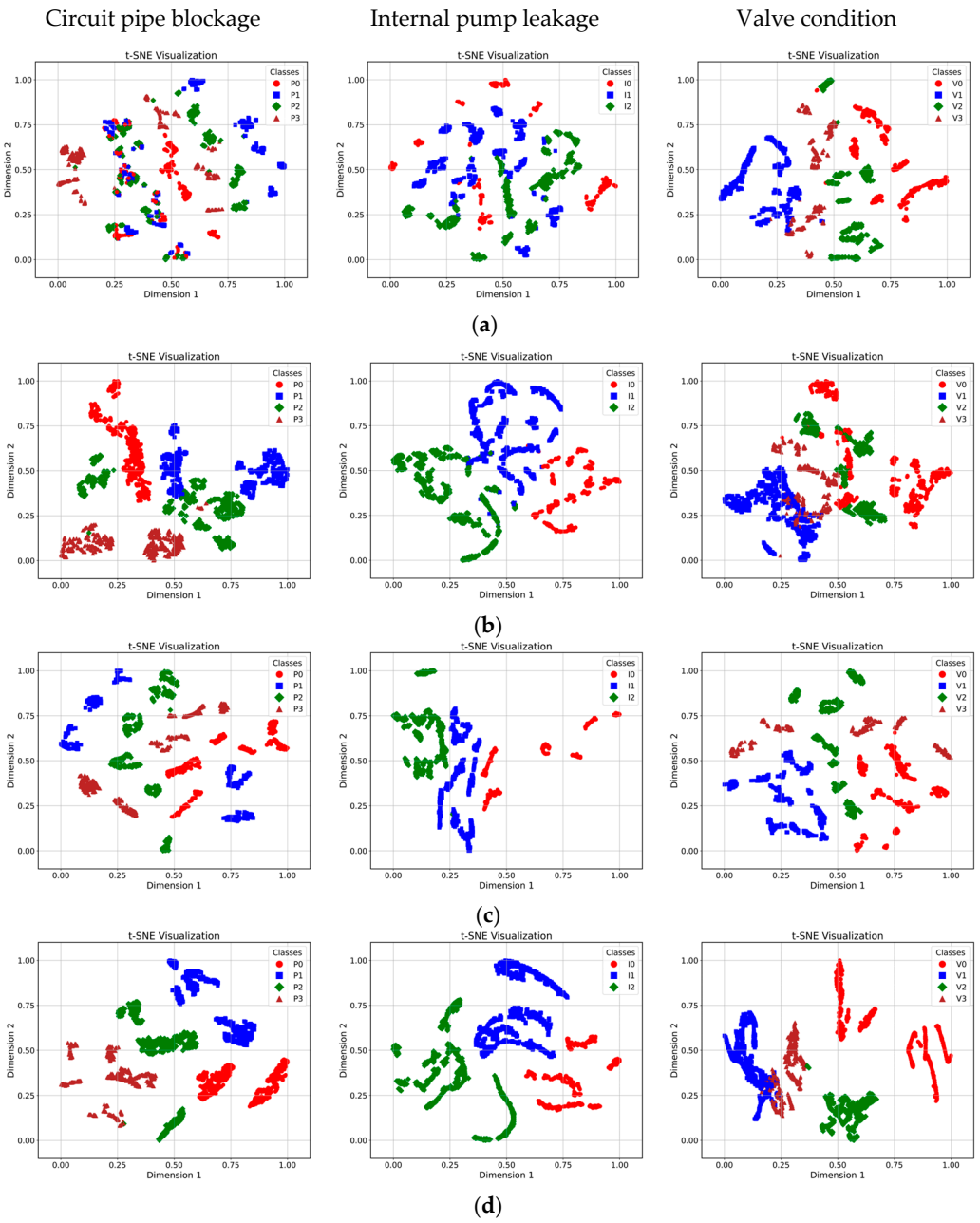


Figure 10. Performance of the CNN-BiLSTM-GAM model: (**a**) CNN output layer; (**b**) BiLSTM layer; (**c**) GAM layer; and (**d**) FC layer.

In this section, the ROC curve is presented along with the corresponding AUC values to assess the diagnostic performance in identifying fault severity, as illustrated in Figure 11. The AUC, representing the area under the ROC curve and ranging from 0.1 to 1, provides a quantitative measure of the model's predictive accuracy. A higher AUC value indicates greater prediction accuracy. The severity recognition accuracies for circuit pipe blockage, internal pump leakage and valve condition approach 100%, with the lowest accuracy exceeding 94%. The results further confirm that the CNN-BiLSTM-GAM model maintains strong stability and high robustness under variable load conditions, especially following sensor layout optimization, thereby outperforming the CNN-GAM model.

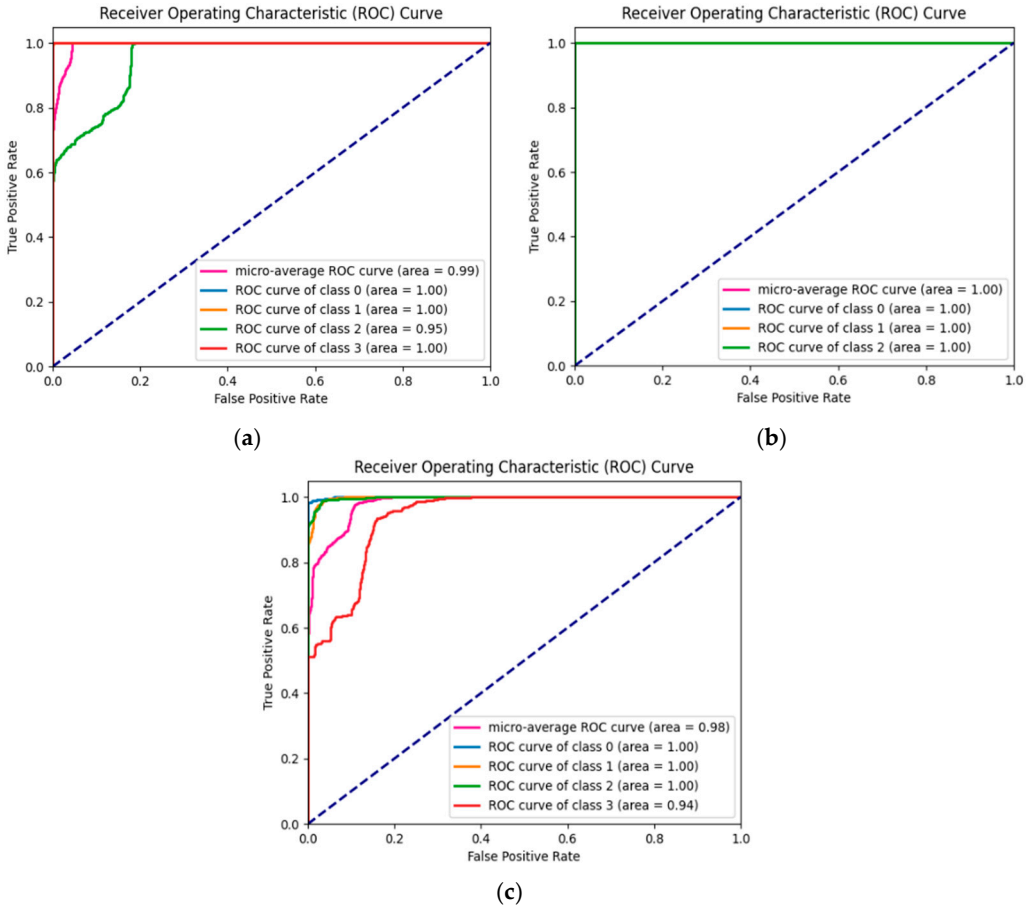


Figure 11. ROC curves of fault severities under test data: (**a**) circuit pipe blockage; (**b**) internal pump leakage; and (**c**) valve condition.

4.3. Comparison with Other Approaches

In this study, the proposed model achieves exceptional computational efficiency of approximately 1.2 million FLOPs per sample, striking an optimal balance between model capacity and computational performance. The architecture demonstrates remarkable engineering practicality by simultaneously fulfilling the stringent requirements for real-time fault diagnosis while maintaining superior classification accuracy across diverse loading conditions.

To thoroughly validate the superior performance of the proposed model, a comprehensive comparative analysis with existing studies was conducted. The research primarily focuses on identifying multiple fault types with varying severity levels in CJ systems operating under diverse working conditions, with particular emphasis on characterizing subtle fault manifestations under diverse operations. The developed model exhibits exceptional generalization capability, demonstrating robust diagnostic performance not only under full-load conditions but also in detecting faint fault signatures during half-load operations. To enhance the practical engineering relevance, a dedicated CJ fault simulation test rig was constructed. Furthermore, ablation studies were systematically performed under half-load conditions to rigorously validate the model's effectiveness. Detailed comparative results are presented in Table 3.

Table 3. Comparison with other models.

Approaches	Dataset	Diagnostic Accuracy		
		Pipe	Pump	Valve
1DCNN [33]	public dataset	-	98.98%	100%
CNN-MAE [14]	public dataset	-	97%	-
BO-LeNet 5 [34]	public dataset	-	99.51%	-
CNN-BiLSTM	diverse load	87.03%	95.21%	93.74%
CNN-GAM	diverse load	93.22%	93.08%	89.65%
Proposed CNN-BiLSTM-GAM	**diverse load**	**99.93%**	**100%**	**98.10%**

5. Conclusions

In conclusion, the real-time fault diagnosis method based on multi-scale feature fusion proposed in this paper has practical application significance for the accurate identification of different fault modes and maintenance of the mooring CJ hydraulic system under variable load conditions. The experimental results demonstrate the following:

1. This study developed the fault diagnosis models based on the CNN-GAM and CNN-BiLSTM-GAM, utilizing multivariate time-series data collected under full-load conditions of the mooring CJ. The t-SNE visualizations of feature outputs at each layer, combined with the accuracy curves, clearly demonstrate the superior ability of the CNN-BiLSTM-GAM model to fuse multi-scale fault features. Additionally, the CNN-BiLSTM-GAM model shows enhanced robustness in handling varying fault conditions.
2. Considering the actual sensor layout of the system, a GAM is applied to calculate and filter the weights across different time steps and all sensors. This study selects pressure sensors PS1, PS3, PS4, PS8, PS10 and PS11; temperature sensors TS3, TS4, TS5, TS10 and TS11; and flow sensors FS2, FS3 and FS4 as inputs for the test model. The proposed approach improves the efficiency of multi-scale feature fusion and optimizes the sensor layout of the system.
3. Under half-load conditions of the CJ, the CNN-BiLSTM-GAM model, utilizing weighted multivariate time series from selected sensors, achieved 99.34% diagnostic accuracy. The results further highlight the superior generalization ability of the CNN-BiLSTM-GAM model, which accurately identifies the severity of circuit pipe blockage, proportional solenoid valve conditions and internal pump leakage.

The proposed CNN-BiLSTM-GAM method is significant for the maintenance and operation of spread mooring systems, marking a critical step toward ensuring safer and more efficient operations of FPSO.

Author Contributions: Conceptualization, Y.L., W.L. and L.H.; methodology, Y.L., W.L. and L.H.; software, Y.L.; validation, Y.L.; formal analysis, Y.L. and W.L.; investigation, Y.L. and L.H.; resources, W.L. and L.H.; data curation, Y.L., W.L., S.L. and H.Y.; writing—original draft preparation, Y.L.; writing—review and editing, Y.L., W.L., S.L. and H.Y.; visualization, Y.L., W.L., S.L. and H.Y.; supervision, W.L.; project administration, W.L., S.L., H.Y. and L.H.; funding acquisition, W.L., S.L. and L.H. All authors have read and agreed to the published version of the manuscript.

Funding: This research was funded by the National Science and Technology Major Project of China (2024ZD140330607), LiaoNing Revitalization Talents Program (XLYC2402020), Dalian Science and Technology Innovation Fund Plan (2024JJ11PTOO4), Excellent teaching Achievement Cultivation Project of Dalian Maritime University (YCG-Z2024001), 111 Project (B18009) and Fundamental Research Funds for the Central Universities (3132023510).

Data Availability Statement: The data presented in this study are available on request from the corresponding author as the data are not publicly available due to privacy and confidentiality considerations.

Conflicts of Interest: Author Lei Hong was employed by the company Nantong Liwei Machinery Co., Ltd. The remaining authors declare that the research was conducted in the absence of any commercial or financial relationships that could be construed as potential conflicts of interest.

References

1. Xu, X.; Gaidai, O.; Naess, A.; Sahoo, P. Improving the prediction of extreme FPSO hawser tension, using another highly correlated hawser tension with a longer time record. *Appl. Ocean Res.* **2019**, *88*, 89–98. [CrossRef]
2. Gaidai, O.; Sun, J.; Cao, Y. FPSO/FLNG mooring system evaluation by Gaidai reliability method. *J. Mar. Sci. Technol.* **2024**, *29*, 546–555. [CrossRef]
3. Wudtke, D.J. Mooring Chain Handling & Tensioning System for FPSO. In Proceedings of the Offshore Technology Conference Brasil, Rio de Janeiro, Brazil, 4–6 October 2011; p. OTC-22273-MS. [CrossRef]
4. Grindheim, R. Movable Chain Jacks and Winches, Case Study of Petrobras' P58/P62 and Eni's Goliat FPSOs. In Proceedings of the Offshore Technology Conference Brasil, Rio de Janeiro, Brazil, 29–31 October 2013; p. OTC-24346-MS. [CrossRef]
5. Wang, A.M.; Yuan, R.; Zhu, S.; Li, H.; Xie, W.; He, M. A Challenging Mating Operation Between VLCC Class FPSO and Soft Yoke Mooring System in Extremely Shallow Water. In Proceedings of the Offshore Technology Conference, Houston, TX, USA, 30 April–3 May 2012; p. OTC-23304-MS. [CrossRef]
6. Biggerstaff, G.; Keith, E.; Taylor, B.; Taylor, M.; Malarchick, A. Lucius Offshore Installation of Flowlines, Risers and Topsides. In Proceedings of the Offshore Technology Conference, Houston, TX, USA, 4–7 May 2015; p. OTC-26042-MS. [CrossRef]
7. Sablok, A.; Blundon, A.; Landbo, T.; Kyoung, J.; Fowlow, C.; Stromme, S. Disconnectable Concrete Spar FPSO. In Proceedings of the OTC Arctic Technology Conference, St. John's, NL, Canada, 24–26 October 2016; p. OTC-27467-MS. [CrossRef]
8. Wu, Y.; Wang, T.; Ma, K.-t.; Heyl, C.; Garrity, R.; Shelton, J. Mooring Tensioning Systems for Offshore Platforms: Design, Installation, and Operating Considerations. In Proceedings of the Offshore Technology Conference, Houston, TX, USA, 30 April–3 May 2018; p. D011S004R004. [CrossRef]
9. Johnson, D.P.; Heyl, C.N.; Kamal, R.; Li, Y. Vito Project: Hull/Mooring Design & Platform Installation. In Proceedings of the Offshore Technology Conference, Houston, TX, USA, 1–4 May 2023; p. D021S023R004. [CrossRef]
10. Pu, H.; Teng, S.; Xiao, D.; Xu, L.; Luo, J.; Qin, Y. Domain generalization for machine compound fault diagnosis by Domain-Relevant Joint Distribution Alignment. *Adv. Eng. Inform.* **2024**, *62*, 102771. [CrossRef]
11. Suo, M.; Xing, J.; Ragulskis, M.; Dong, Y.; Zhang, Y.; Lu, C. Fault diagnosis of satellite power system based on unsupervised knowledge acquisition and decision-making. *Adv. Eng. Inform.* **2024**, *62*, 102768. [CrossRef]
12. Ye, H.; Li, W.; Lin, S.; Ge, Y.; Lv, Q. A framework for fault detection method selection of oceanographic multi-layer winch fibre rope arrangement. *Measurement* **2024**, *226*, 114168. [CrossRef]
13. Wang, H.; Zhou, J.; Chen, H.; Xu, B.; Shen, Z. Hydraulic system fault diagnosis decoupling method based on 2D time-series modeling and self-attention fusion. *Sci. Rep.* **2024**, *14*, 15620. [CrossRef]
14. Chen, X.; Liu, H.; Nikitas, N. Internal pump leakage detection of the hydraulic systems with highly incomplete flow data. *Adv. Eng. Inform.* **2023**, *56*, 101974. [CrossRef]
15. Zhu, Y.; Zhou, T.; Tang, S.; Yuan, S. Failure analysis and intelligent identification of critical friction pairs of an axial piston pump. *J. Mar. Sci. Eng.* **2023**, *11*, 616. [CrossRef]
16. Xia, M.; Li, T.; Xu, L.; Liu, L.; De Silva, C.W. Fault diagnosis for rotating machinery using multiple sensors and convolutional neural networks. *IEEE/ASME Trans. Mechatron.* **2017**, *23*, 101–110. [CrossRef]
17. Gong, W.; Chen, H.; Zhang, Z.; Zhang, M.; Wang, R.; Guan, C.; Wang, Q. A novel deep learning method for intelligent fault diagnosis of rotating machinery based on improved CNN-SVM and multichannel data fusion. *Sensors* **2019**, *19*, 1693. [CrossRef]
18. Wu, C.; Jiang, P.; Ding, C.; Feng, F.; Chen, T. Intelligent fault diagnosis of rotating machinery based on one-dimensional convolutional neural network. *Comput. Ind.* **2019**, *108*, 53–61. [CrossRef]
19. Xue, F.; Zhang, W.; Xue, F.; Li, D.; Xie, S.; Fleischer, J. A novel intelligent fault diagnosis method of rolling bearing based on two-stream feature fusion convolutional neural network. *Measurement* **2021**, *176*, 109226. [CrossRef]
20. Hao, S.; Ge, F.-X.; Li, Y.; Jiang, J. Multisensor bearing fault diagnosis based on one-dimensional convolutional long short-term memory networks. *Measurement* **2020**, *159*, 107802. [CrossRef]
21. Ma, R.; Zhao, H.; Wang, K.; Zhang, R.; Hua, Y.; Jiang, B.; Tian, F.; Ruan, Z.; Wang, H.; Huang, L. Leakage fault diagnosis of lifting and lowering hydraulic system of wing-assisted ships based on WPT-SVM. *J. Mar. Sci. Eng.* **2022**, *11*, 27. [CrossRef]
22. Liu, Y.; Li, W.; Lin, S.; Zhou, X.; Ge, Y. Hydraulic system fault diagnosis of the chain jacks based on multi-source data fusion. *Measurement* **2023**, *217*, 113116. [CrossRef]

23. Yang, X.; Jiang, A.; Jiang, W.; Yue, Y.; Jing, L.; Zhou, J. Small-Sample Fault Diagnosis of Axial Piston Pumps across Working Conditions, Based on 1D-SENet Model Migration. *J. Mar. Sci. Eng.* **2024**, *12*, 1430. [CrossRef]
24. Tao, H.; Jia, P.; Wang, X.; Wang, L. Real-Time Fault Diagnosis for Hydraulic System Based on Multi-Sensor Convolutional Neural Network. *Sensors* **2024**, *24*, 353. [CrossRef]
25. Jiang, J.; Li, H.; Mao, Z.; Liu, F.; Zhang, J.; Jiang, Z.; Li, H. A digital twin auxiliary approach based on adaptive sparse attention network for diesel engine fault diagnosis. *Sci. Rep.* **2022**, *12*, 675. [CrossRef]
26. Ji, S.; Yu, D.; Shen, C.; Li, W.; Xu, Q. Landslide detection from an open satellite imagery and digital elevation model dataset using attention boosted convolutional neural networks. *Landslides* **2020**, *17*, 1337–1352. [CrossRef]
27. Huang, B.; Liang, Y.; Qiu, X. Wind power forecasting using attention-based recurrent neural networks: A comparative study. *IEEE Access* **2021**, *9*, 40432–40444. [CrossRef]
28. Wang, H.; Liu, Z.; Peng, D.; Qin, Y. Understanding and learning discriminant features based on multiattention 1DCNN for wheelset bearing fault diagnosis. *IEEE Trans. Ind. Inform.* **2019**, *16*, 5735–5745. [CrossRef]
29. Shao, Z.; Yin, Y.; Lyu, H.; Soares, C.G.; Cheng, T.; Jing, Q.; Yang, Z. An efficient model for small object detection in the maritime environment. *Appl. Ocean Res.* **2024**, *152*, 104194. [CrossRef]
30. Wu, K.; Wu, J.; Feng, L.; Yang, B.; Liang, R.; Yang, S.; Zhao, R. An attention-based CNN-LSTM-BiLSTM model for short-term electric load forecasting in integrated energy system. *Int. Trans. Electr. Energy Syst.* **2021**, *31*, e12637. [CrossRef]
31. Gao, J. Network intrusion detection method combining CNN and BiLSTM in cloud computing environment. *Comput. Intell. Neurosci.* **2022**, *2022*, 7272479. [CrossRef]
32. Long, Z.; Zhang, X.; Zhang, L.; Qin, G.; Huang, S.; Song, D.; Shao, H.; Wu, G. Motor fault diagnosis using attention mechanism and improved adaboost driven by multi-sensor information. *Measurement* **2021**, *170*, 108718. [CrossRef]
33. Prakash, J.; Miglani, A.; Kankar, P.K. Internal Leakage Detection in Hydraulic Pump Using Model-Agnostic Feature Ranking and Ensemble Classifiers. *J. Comput. Inf. Sci. Eng.* **2023**, *23*, 041005. [CrossRef]
34. Tang, S.; Zhu, Y.; Yuan, S. An adaptive deep learning model towards fault diagnosis of hydraulic piston pump using pressure signal. *Eng. Fail. Anal.* **2022**, *138*, 106300. [CrossRef]

Disclaimer/Publisher's Note: The statements, opinions and data contained in all publications are solely those of the individual author(s) and contributor(s) and not of MDPI and/or the editor(s). MDPI and/or the editor(s) disclaim responsibility for any injury to people or property resulting from any ideas, methods, instructions or products referred to in the content.